A Framework for Understanding Displacement Damage Mechanisms in Irradiated Silicon Devices

J. R. Srour, *Fellow, IEEE*, and J. W. Palko

***Abstract*—A framework is presented for understanding carrier generation and recombination mechanisms in irradiated silicon devices. Data obtained by many workers for irradiated bulk material and devices are analyzed and summarized, and key damage-factor dependences are identified. Measurements, simulations, and analyses support the conclusion that correlation of displacement damage effects with the rate of nonionizing energy loss (NIEL) for proton, neutron, pion, and heavy-ion bombardment is due to the dominant influence of defect subclusters. At low NIEL values ($< 5 \times 10^{-5}$ MeV-cm^2/g), isolated defects dominate the electrical properties. At relatively high NIEL ($>2 \times 10^{-4}$ MeV-cm^2/g), subclusters dominate. Enhanced carrier generation and recombination produced by those small disordered regions is considered. Modeling results are presented for behavior observed in the transition region between domination by isolated defects and by clusters. The model presented in this paper simultaneously accommodates defect cluster models and NIEL scaling phenomena in the same framework.**

***Index Terms*—Clusters, defects, displacement damage, NIEL, radiation effects, silicon.**

I. Introduction

THIS paper presents a framework to aid the mechanistic understanding of displacement damage effects in irradiated Si devices. Emphasis is placed on the most important displacement-damage mechanisms in devices: increased carrier recombination and carrier generation due to radiation-induced levels in the Si bandgap. We have critically examined literature data, analyses, and simulations and performed new analyses and simulations, then used the results to develop a model that simultaneously includes defect clusters, as defined below, and the more recently emphasized NIEL scaling phenomena. (NIEL is the rate of nonionizing energy loss per unit distance traveled in a Si device by an incident particle.) The need for an encompassing model was noted in [1].

The approach used in this paper is to address carrier generation at radiation-induced centers first then to examine carrier recombination, which is more complex. A model for recombination is presented that builds on the generation model described herein.

The key argument presented is that NIEL scaling of carrier generation and recombination processes, which is commonly observed at relatively high NIEL values (i.e., $>2 \times 10^{-4}$ MeV-cm^2/g, with an example particle in that range being 100-MeV protons), is due to the dominant effects of defect subclusters. In the present description, NIEL scaling also occurs at relatively low NIEL values (i.e., $< 5 \times 10^{-5}$ MeV-cm^2/g, with an example particle in that range being 1-MeV electrons) and is due solely to the effects of isolated defects. Behavior in the transition NIEL regime from isolated-defect to subcluster dominance is modeled in terms of the increasing effect of subclusters with increasing NIEL. Saturation is reached at relatively high NIEL values where the number of subclusters produced increases linearly with NIEL. In that regime, damage factors for generation and recombination become invariant with NIEL.

The work presented herein focuses primarily on the experimental situation in which NIEL is relatively constant with penetration depth, i.e., the case of incident high-energy monoenergetic particles with ranges in Si that are much larger than the irradiated device thickness. NIEL can then be interpreted as the displacement damage dose (D_d) deposited per unit particle fluence.

The terms "cluster" and "subcluster" are used interchangeably in this paper, and both mean the small defect regions produced at the end of ion tracks. Neither of those terms should be confused with the early concept of a defect cluster that referred to a relatively large region encompassing all the defects produced by an energetic displaced Si ion. The importance of clusters in irradiated Si has been questioned occasionally in the literature by some workers. In contrast, other workers have continued to use clusters in accounting for experimental findings. The present framework attempts to clarify those differing views.

II. Generation at Radiation-induced Centers

A. Data Description

Generality is evident when data for thermal generation of electron-hole pairs at radiation-induced centers are examined in detail. Previously [2], it was demonstrated that the radiation-induced increase in thermal generation rate per unit depletion-region volume (ΔG) per unit deposited nonionizing dose, D_d, in all irradiated Si devices is independent of NIEL for all incident particle types and energies except those that primarily produce relatively isolated defects (e.g., low-energy electrons). (D_d is given by the product of NIEL and particle fluence.) A model to explain that universal behavior is described herein.

Fig. 1 shows the information presented in [2], which demonstrates linear scaling of ΔG per unit fluence with NIEL. $K_{\rm dark}$, the dark-current damage factor, is defined as $\Delta G/D_d$. The universal value of $K_{\rm dark}$ at high NIEL, 1.9×10^5 carriers/cm^3-sec per MeV/g, applies for incident protons, neutrons, pions, and heavy ions of all energies and,

Manuscript received July 14, 2006; revised September 10, 2006. This work was supported by The Aerospace Corporation.

The authors are with the Aerospace Corporation, Los Angeles, CA 90009 USA.

Digital Object Identifier 10.1109/TNS.2006.885796

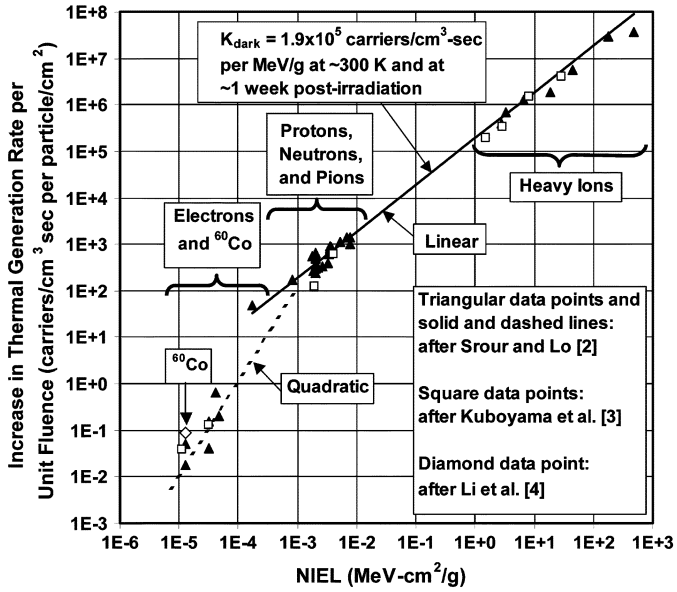

Fig. 1. Radiation-induced increase in thermal generation rate per unit fluence (= K_{dark} x NIEL) versus the displacement damage dose deposited per unit fluence (= NIEL). Proton and electron NIEL values used in plotting the data of Kuboyama *et al.* [3] were obtained from [17] instead of using the NIEL values given in [3].

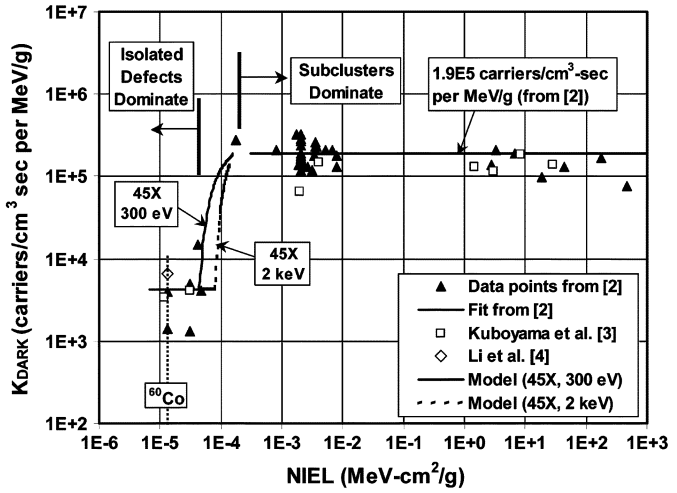

Fig. 2. Replot of Fig. 1 in terms of dark-current damage factor versus NIEL. Results of model calculations are shown for the low-NIEL regime.

more generally, for all irradiations with particles with NIEL greater than $\sim 2 \times 10^{-4}$ MeV-cm^2/g. In that regime, $K_{\rm dark}$ is independent of dopant and impurity type and concentration [2]. Fig. 1 also shows data obtained by Kuboyama [3] and Li [4] that are consistent with the findings in [2].

Fig. 2 shows $K_{\rm dark}$ versus NIEL (derived from Fig. 1), which clearly illustrates that NIEL scaling occurs at higher NIEL values (i.e., a constant value of $K_{\rm dark}$). The apparent quadratic dependence of ΔG at low NIEL values, indicated in Fig. 1, would map to a linear dependence if shown in Fig. 2. However, the scatter in the data in that regime in Fig. 1 suggests that a simple quadratic dependence may be inappropriate for modeling and interpreting the generation data, as discussed later.

Fig. 2 demonstrates that radiation-induced carrier generation is much more effective per unit deposited dose at high NIEL than at low NIEL (i.e., $K_{\rm dark}$ is much larger). For neutron bombardment, Watts [5] and Gill [6] proposed a model of enhanced generation due to the close proximity of radiation-induced defects in subclusters based on enhanced carrier *recombination* modeling [7]–[9]. They obtained a 1-MeV-neutron to ^{60}Co-photon generation enhancement ratio on the order of 100 through measurements and analyses. In Figs. 1 and 2, the ratio of $K_{\rm dark}$ at high NIEL to that at low NIEL for ^{60}Co damage is roughly comparable to their results. Generation and recombination enhancement are considered in more detail below. First, we explore physical explanations for the universal behavior evident in Figs. 1 and 2 at high NIEL values.

B. Clustered and Isolated Defects

Wood [10] and More [11] performed displacement damage simulations and measurements that are relevant to the present modeling. Their key finding is that, for a given primary knock-on atom (PKA) of sufficient energy, the ratio of the energy deposited into the production of defects contained in subclusters $(E_{\rm clus})$ to the energy deposited into the production of isolated defects $(E_{\rm iso})$ is essentially constant and independent of PKA energy. NIEL scaling of ΔG is now examined in view of their results.

Depending on sample dimensions, particle type, and particle energy, an incident particle may produce one or more Si PKAs. The PKA energy spectrum also varies with particle type and energy. Wood and More determined that there is an upper bound to the PKA energy beyond which the knock-on atom produces subsidiary knock-on atoms that themselves obey the partitioning of energy between clustered and isolated defect production. There is a small range for the total kinetic energy of recoils ($\sim$1.6–12 keV in the Wood work) for which *individual* subclusters are produced, which is reasonably represented here by a single average value, $\bar{E}_{\rm clus}$. (Ionization losses are negligible at that energy, but must be considered for higher energy recoils and are taken into account in Wood and More's results as well as in our calculations of energy partitioning for high-energy PKAs.) The *total* energy deposited into subcluster production can then be expressed as $E_{\rm clus} = N_{\rm clus}\bar{E}_{\rm clus}$, where $N_{\rm clus}$ is the total number of subclusters created for a given fluence.

Based on the constant ratio for energy partitioning between clustered and isolated defects, it is readily shown that the *total* energy deposited into *all* displacements is given by $E_{\rm tot} \cong E_{\rm clus}/f_{\rm clus}({\rm sat})$ where $f_{\rm clus}({\rm sat})$ is that fraction of the total displacement energy deposited into subcluster production at high NIEL (i.e., $>2 \times 10^{-4}$ MeV-cm^2/g). In that regime, $f_{\rm clus}({\rm sat})$ is essentially constant (or saturated). (For lower NIEL values, the fraction of energy deposited into subclusters is variable, and we denote that parameter as $f_{\rm clus}$ in Section II-C.) From the assumption of nearly constant NIEL with penetration depth, we obtain $E_{\rm tot} \propto ({\rm NIEL})(W)$, where W is the material thickness of interest. Combining expressions yields $N_{\rm clus} \propto ({\rm NIEL})(W)(f_{\rm clus}({\rm sat}))/\bar{E}_{\rm clus}$, or $N_{\rm clus} \propto$ NIEL; i.e., the number of subclusters produced is proportional to NIEL

provided that the NIEL value is large enough for the energy loss to exhibit constant energy partitioning.

For unity fluence, $K_{\rm dark}$ equals $\Delta G/{\rm NIEL}$. At relatively high NIEL, as the number of subclusters increases, the thermal generation rate will increase in proportion to the addition of generation centers. Thus, since that number increases linearly with NIEL, then ΔG will also increase linearly, which results in a constant value for $K_{\rm dark}$, in agreement with data in [2] (shown here in Fig. 2). For relatively low NIEL (e.g., $< 5 \times 10^{-5}$ MeV-cm^2/g), as NIEL increases the number and density of isolated defects produced by a single incident particle will increase because more nonionizing dose is deposited. Once a NIEL value is reached that is sufficient to produce energetic PKAs, subclusters are created in addition to isolated defects. This will occur at electron energies roughly > 5 MeV.

In subclusters, the much higher defect density present evidently dominates thermal generation as compared to the isolated defects that dominate at low NIEL values. For relatively high NIEL ($>2\times10^{-4}$ MeV-cm^2/g), $K_{\rm dark}$ becomes essentially constant since subclusters with very similar properties dominate. In that regime, where both isolated *and* clustered defects are produced, the increase in ΔG is attributed here to dominance by subclusters and not to radiation-induced isolated defects based on the finding in [2] that no dopant type or impurity dependence is evident for $K_{\rm dark}$ at high NIEL. The defect density in a subcluster is much greater than that for dopant atoms and impurities in Si, so the intrinsic radiation-induced defects in a subcluster will dominate. If isolated defects were dominant, then a universal damage factor would not have been obtained. (This statement is based primarily on *recombination* data, which are discussed in Section III. Those data clearly show a significant dependence on dopant type and impurities at low NIEL. For the *generation* case, we believe a similar conclusion is likely to hold at low NIEL, but there is insufficient data at present to make that conclusion.)

The key point employed here from the Wood and More work is that the ratio of the displacement energy deposited in producing subclusters to that deposited in producing isolated defects is a constant for all PKA energies [10], [11]. For radiation-induced increases in dark current, NIEL scaling is explained in terms of subclusters dominating device behavior. That is, *NIEL scaling follows directly from the presence and dominance of defect subclusters at high NIEL.* (Note that linear scaling of the increase in ΔG with NIEL (Fig. 1) maps to a constant value of $K_{\rm dark}$ (Fig. 2). Thus, in the present work, NIEL scaling means a constant damage factor in a specific NIEL regime.) Section II-C describes our modeling results, which include NIEL scaling at low NIEL as well due to a linear increase in isolated defect production in that regime.

Mueller *et al.* [12] suggested that the end-of-track structure is similar for all damage cascades in irradiated Si and generally consists of 2 to 3 subclusters, regardless of the initial PKA energy. They also suggested that the additional energy deposited into displacement damage produces only isolated defects along the earlier portion of the track, which increases in length with PKA energy. Such suggestions are not compatible with simulations of recoil-atom energy spectra in irradiated Si. Molecular dynamics (MD) simulations of implanted Si ions in Si (e.g., [13] and [14]) have shown that both primary *and* secondary recoils with energy on the order of 500 eV or greater consistently produce damage cascades and clustered defects. The Mueller work appears to disagree with the simulations of Wood [10] and More [11] that show a significant increase with increasing PKA energy in the displacement damage energy deposited into subcluster production by high-energy secondary recoils. We conducted BCA (binary collision approximation) simulations of Si atoms impinging on an amorphous Si target using the SRIM code [15] and obtained results that confirm the Wood and More findings.

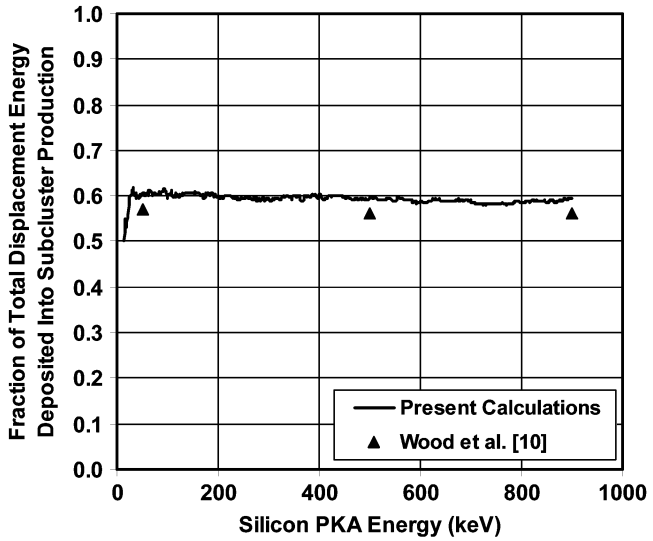

Fig. 3. Results of Monte-Carlo calculations of the partitioning of displacement-damage energy deposited into subcluster and isolated-defect formation. Shown is that fraction of the total displacement energy deposited into subcluster production. Also shown are results of Wood *et al.* [10]. The lack of a dependence on primary recoil energy confirms their findings and those of More [11].

We also replicated the Monte Carlo calculations of direct and indirect spectra made by Wood and More. Results are shown in Fig. 3, which confirms that the ratio of the energy deposited into producing subclusters to that deposited into creating isolated defects is essentially independent of primary recoil energy in silicon. Shown is the fraction of the total displacement energy deposited into subclusters, with the average value being 0.59. Wood [10] obtained 0.57 for that fraction based on calculations made at three PKA energies, as illustrated. This constant energy partitioning depends on the existence of a bounded region for single cluster creation, as established by Wood [10] and More [11], and on an apparent invariance with PKA energy of the relative probability of recoils having an energy in that single-cluster formation regime versus having an energy in the isolated-defect formation regime.

This partitioning is based on complete stopping of Si recoils. Thus, our analysis is strictly only applicable for equilibrium recoil spectra, such that scatter-in and scatter-out from the active region cancel each other. Weller [16] developed the concept of nonionizing energy deposition rate (NIEDR), which gives the depth derivative of final displacement energy deposition. NIEDR may be a useful tool for clarifying the effects of device geometries that allow unbalanced escape of recoils on the partitioning of isolated versus clustered damage. In our Monte Carlo

calculations, we only considered cases where nuclear interactions are unimportant since those interactions are not included in SRIM. The majority of the experimental data considered here also falls into that category.

C. Modeling of Behavior in the Transition NIEL Regime

The partitioning of energy into the production of subclusters and isolated defects for energetic electron bombardment is considered here to model $K_{\rm dark}$ in the transition NIEL regime from $\sim 5\times 10^{-5}$ to $\sim 2\times 10^{-4}$ MeV-cm^2/g (Fig. 2). The displacement energy associated with an incident electron may be obtained by integrating the probability distribution of interactions producing recoils of a certain energy. The probability is based on the displacement cross section $\sigma(T_e, T_r)$ for a recoil of kinetic energy T_r produced by an incident electron of kinetic energy T_e. The rate of nonionizing energy loss for electrons incident on silicon was calculated here as a function of electron energy using the method described by Summers [17].

The partitioning of energy deposited into displacement damage at higher and lower electron energies is important in understanding degradation mechanisms. Here the terms *higher* and *lower* refer to energies that are sufficient to form subclusters and those that are not, respectively. The ratio of energy deposited in those regimes was evaluated by splitting the NIEL integral given in [17] into two corresponding parts. Such a division is identical to the method used by Wood [10] and More [11] in determining their direct spectrum. Because of the relatively low energy of the recoils generally produced by incident electrons, the simplifying assumption is made here that all the energy deposited in events above T_L goes into subcluster formation and that none of it is repartitioned into creating isolated defects, where T_L is the lower limit for recoil energies that create a subcluster.

As discussed above, the numbers of defects in both the clustered and isolated defect regimes are proportional to the damage energy deposited in those regimes. Using enhancement factors experimentally measured for damage occurring at high and low NIEL, we can estimate the functional form for the recombination and generation damage factors (i.e., $K_{\rm rec}$, which is defined and discussed in Section III, and $K_{\rm dark}$, both of which are denoted by K in this section) in the transition regime from purely isolated defects to clustered defects. For the generation example, the radiation-induced increase in generation rate can be expressed as

$$\Delta G \propto R_m E_{\rm clus} + E_{\rm iso} \tag{1}$$

where R_m is the relative *microscopic* effectiveness, per unit deposited energy, of clusters with respect to isolated defects in causing carrier generation (or recombination). We can express energy fractions in the following way: $E_{\rm clus} = (f_{\rm clus})(E_{\rm tot})$ and $E_{\rm iso} = (f_{\rm iso})(E_{\rm tot})$, where $f_{\rm iso}$ and $f_{\rm clus}$ are the fractions of the total damage energy $(E_{\rm tot})$ deposited into the production of isolated defects and subclusters, respectively (i.e., $f_{\rm iso} + f_{\rm clus} = 1$). (Note that $f_{\rm iso}$ and $f_{\rm clus}$ are variable in the transition region.) Dividing (1) by total nonionizing energy loss to give the fraction of energy deposited into each defect category yields

$$K \propto R_m f_{\rm clus} + f_{\rm iso} = 1 + f_{\rm clus}(R_m - 1). \tag{2}$$

At low NIEL values where purely isolated defects are responsible for carrier generation (and recombination), the right-hand side of this expression becomes unity. As shown in [17], $f_{\rm clus}$ will begin to increase with incident particle energy (roughly proportional to NIEL in this regime) as recoils with energy above T_L become possible. Eventually, with increasing NIEL, $f_{\rm clus}$ will saturate as discussed in Section II-B, so that K will have a roughly sigmoidal shape. The expression for the experimentally determined ratio of K at high NIEL to K at low NIEL, referred to here as the macroscopic high–low effectiveness ratio $R_{\rm hl}$, is then given by

$$R_{\rm hl} = 1 + f_{\rm clus}({\rm sat})(R_m - 1) \tag{3}$$

which holds for the essentially constant, saturated value of $f_{\rm clus}$ that occurs at high NIEL. As an example, using a value for $f_{\rm clus}({\rm sat})$ of 0.59 (from Fig. 3), for the representative case of $R_{\rm hl} = 45$ for carrier generation (based on Fig. 2, as discussed below) we obtain a microscopic generation effectiveness ratio of 76.

Equation (2) was used to generate families of curves as a function of macroscopic enhancement factor, $R_{\rm hl}$, and minimum cluster formation energy, T_L, for the range 0.3 to 2 keV. Curves were then selected to fit experimental data spanning the NIEL range from purely isolated defects created by electrons with energy < 5 MeV to higher electron energies that produce both subclusters and isolated defects. Summers [17] previously determined $f_{\rm iso}$ and $f_{\rm clus}$ for $T_L = 2$ keV in electron-irradiated Si, and described the damage produced in the transition regime as a function of incident energy.

From Fig. 2, a typical experimental value of $\rm R_{hl}$ for carrier generation is 45, as used in the example above. We employed that value and a cluster formation energy of 300 eV to obtain the model fit shown in Fig. 2. (This formation energy is lower than that employed by Wood [10] in Monte Carlo simulations. However, MD simulations reveal that subclusters are produced at PKA energies less than 500 eV [14].) A considerably less successful fit made using an energy of 2 keV is also shown for comparison. The general features of the data appear to be accounted for well by this description, particularly for the case of a cluster formation energy of 300 eV. Qualitatively, the constant value of $K_{\rm dark}$ in the fit at low NIEL is due to a linear increase with NIEL of the number of isolated defects produced; there is no contribution from subclusters since they are not produced in that regime. At high NIEL values, the constant value of $K_{\rm dark}$ is due to the ratio of clustered defects to isolated defects produced being essentially invariant with increasing NIEL. In the transition NIEL regime from approximately 5×10^{-5} to 2×10^{-4} MeV-cm^2/g, the clustered-defect-to-isolated-defect ratio increases with NIEL.

In the preceding modeling, the probability of cluster formation is treated as a strictly binary function of energy. As such, the transition from low to high NIEL behavior is a manifestation of those recoils with energy above the cluster formation threshold.

In reality, there is undoubtedly a gradually increasing probability of cluster formation with recoil energy near this threshold. Such a relation would produce a more gradual transition from low to high NIEL behavior for $K_{\rm dark}$.

III. Recombination at Radiation-Induced Centers

We explored carrier recombination in a manner similar to that employed above for carrier generation. Differences between the two processes include the following dependences for recombination that are absent for generation: injection level; n-type versus p-type; resistivity. Oxygen concentration is also important for recombination at isolated defects. Other dependences, which affect both generation and recombination, include temperature and time after irradiation. We focused on the following common situation: a) B-doped and P-doped Si are considered; b) short-term and long-term thermal annealing effects are not addressed – instead, we consider effects occurring at $\sim$300 K for relatively stable defects; c) injection effects are minimized by primarily considering the low-injection-level regime. Literature data are only considered for bulk Si and Si solar cells (and other diodes) in an attempt to minimize the impact of any device phenomena that might obscure mechanistic insight. Attention is also given to crystal growth method, i.e., Czochralski (CZ) or float zone (FZ), since the oxygen content varies strongly between the two (i.e., CZ: high oxygen; FZ: low oxygen).

Analogous to $K_{\rm dark}$, a general recombination damage factor, $K_{\rm rec}$, is defined here as $\Delta R/D_d$, which equals $\Delta(1/\tau_r)/D_d \cdot$ ΔR is the radiation-induced increase in recombination rate per unit volume per unit excess carrier concentration and $\Delta(1/\tau_r)$ is the radiation-induced increase in reciprocal recombination lifetime. For low-injection-level conditions, recombination lifetime is independent of excess carrier density, as discussed below. Since the recombination rate definition is in terms of *per unit excess carrier density*, that term is eliminated from the definition of $K_{\rm rec}$. $K_{\rm rec}$ is related to common definitions of recombination-lifetime and diffusion-length damage coefficients (K_r and K_l, respectively): $K_{\rm rec}$ equals K_r/NIEL and equals $K_l D$/NIEL, where $K_r = \Delta(1/\tau_r)/\Phi$ and $K_l = \Delta(1/L^2)/\Phi$ (D is diffusivity, L is diffusion length, and Φ is fluence).

Figs. 4–6 show examples of the resistivity dependence of $K_{\rm rec}$ derived from literature data. For neutron bombardment (Fig. 6), the damage factor is essentially independent of resistivity below $\sim$10 ohm-cm, and decreases at higher resistivities. In contrast, for 1-MeV electron bombardment (Fig. 5) $K_{\rm rec}$ continues to increase at low resistivities. The dependence of $K_{\rm rec}$ on resistivity, ρ, for the ^{60}Co and electron cases (Figs. 4 and 5, respectively) is roughly $\rho^{-0.5}$. Differences are also evident between damage factors for bulk samples and for solar cells (discussed below). Also, the effect of oxygen concentration is evident when $K_{\rm rec}$ is compared for FZ and CZ samples. That dependence occurs when isolated defects prevail but not when subclusters dominate.

Fig. 7 shows examples of the injection-level dependence of $K_{\rm rec}$ [20], [26]. Injection effects are quite different when behavior for particles that produce only isolated defects is compared with that for particles that produce subclusters. Note the relatively strong dependence of damage factor on injection ratio

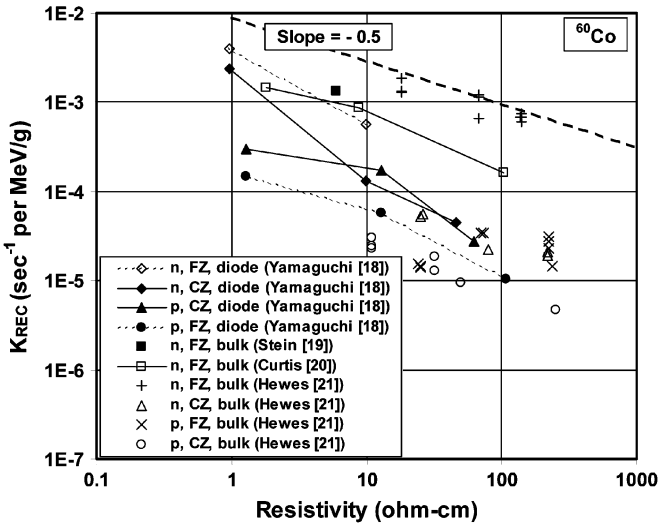

Fig. 4. Resistivity dependence of recombination damage factor for ^{60}Co gamma-irradiated silicon.

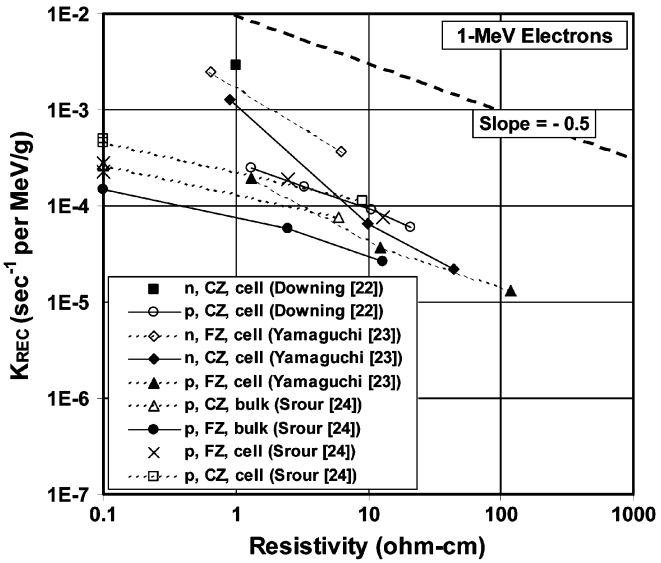

Fig. 5. Resistivity dependence of recombination damage factor for 1-MeV electron-irradiated silicon.

for neutron-irradiated Si and the relatively weak dependence for the case of ^{60}Co gamma-ray bombardment.

Recombination information based on literature data, expressed here in terms of $K_{\rm rec}$, is shown versus NIEL in Fig. 8 for bulk material and solar cells. (Source information for all data points shown in Figs. 8 and 9 is given in Table I.) Similarities between Figs. 2 and 8 are apparent. The main features of Fig. 8 are: 1) At relatively low NIEL values, $K_{\rm rec}$ varies significantly with dopant type, oxygen concentration, and, particularly for p-type material, NIEL. Oxygen concentration effects are especially evident for ^{60}Co gamma-irradiated Si. 2) For relatively high NIEL, all data group together reasonably well. Reasons for the scatter in that regime include: a) $K_{\rm rec}$ is somewhat different for n- and p-type Si when data obtained by the same researcher at the same NIEL value are compared (e.g., Curtis [25] or Gregory [26]); b) differences between

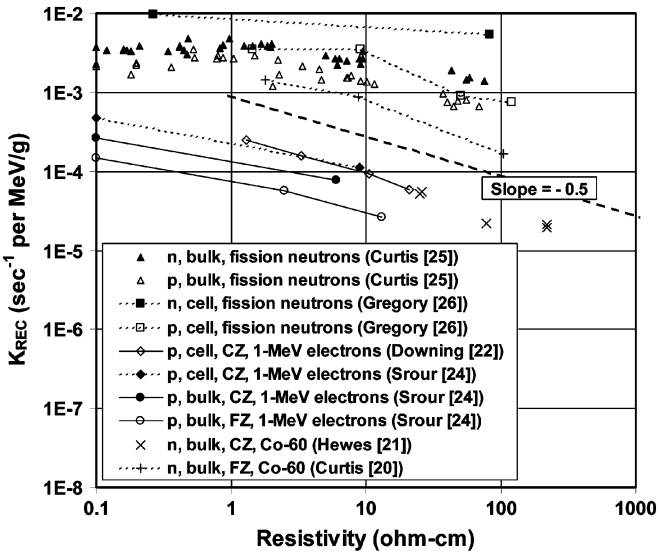

Fig. 6. Comparison of the resistivity dependence of the recombination damage factor for Si irradiated with neutrons, electrons, and gamma rays.

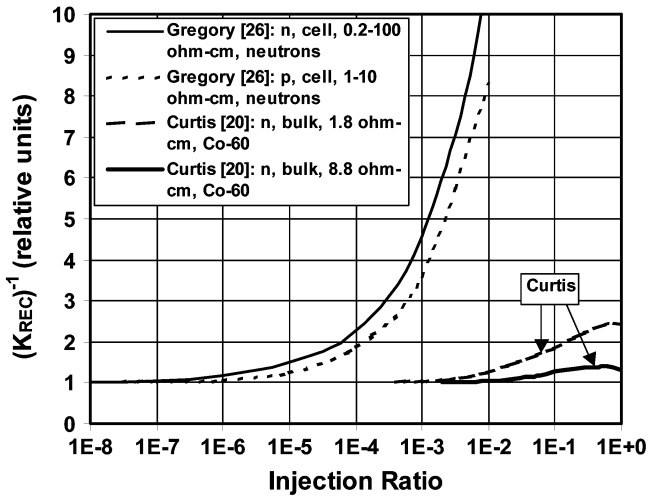

Fig. 7. Comparison of the injection-level dependence of recombination damage factor for neutron- and ^{60}Co gamma-irradiated silicon. Injection ratio is defined as the ratio of the injected-carrier density to the equilibrium majority-carrier density.

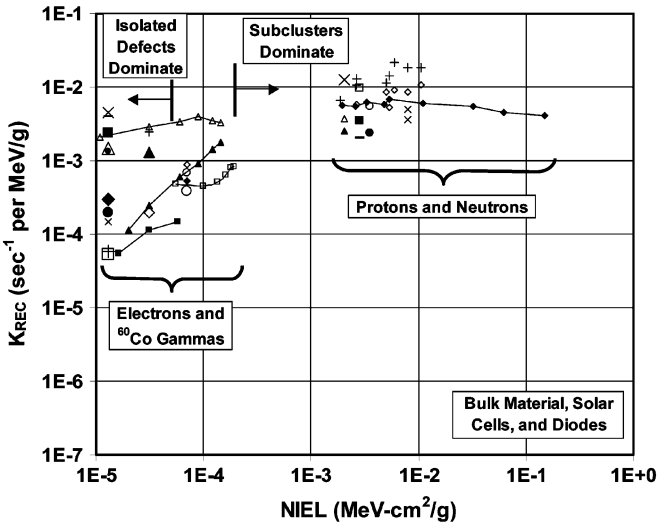

Fig. 8. Recombination damage factor versus NIEL for bulk Si and Si solar cells and diodes irradiated with various particles. Data are for relatively low resistivity samples at relatively low injection levels. Table I gives the source information for the data presented in this figure.

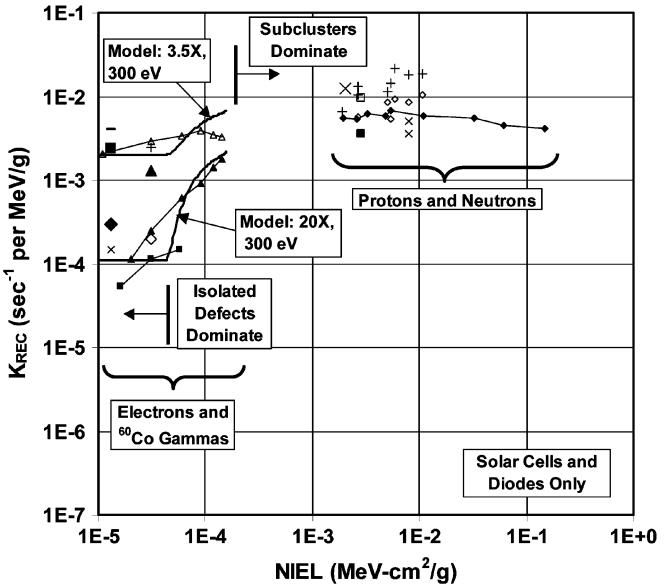

Fig. 9. Recombination damage factor versus NIEL for Si solar cells and diodes irradiated with various particles. Results of model calculations are shown for two cases in the low-NIEL regime. Table I gives the source information for the data presented in this figure.

solar-cell and bulk $K_{\rm rec}$ values are evident (e.g., Curtis [25] versus Gregory [26]).

Systematic differences are often evident between $K_{\rm rec}$ values for bulk material and solar cells. As discussed below, bulk measurements can be influenced by charge trapping effects. In addition, bulk damage factors generally were not determined at the same low injection level as those for solar cells. Because of those differences and the possible confusion that may result, data for solar cells and diodes in Fig. 8 are displayed separately in Fig. 9. Data in the transition NIEL regime are modeled in the same manner as described above for carrier generation. Values for experimentally determined recombination enhancement factors are given in Table II for various cases. Those factors were used to guide the modeling of recombination data. The model fits in Fig. 9 account for the data reasonably well, which indicates that the present mechanistic description is accurate for recombination *and* generation processes.

Fig. 10 presents a representative overview of the present description of recombination processes for the case of relatively low resistivities and low injection levels. For this example, constant damage factors at high NIEL for n- and p-type Si are based on data obtained by Gregory [26] and Othmer [29] for neutron-irradiated devices. (Damage-factor differences between n- and p-type Si at high NIEL have been measured by several workers [25], [26], [30], [32], [33], and that topic is considered further in Section IV-C.) Constant damage factors at low NIEL emphasize Yamaguchi's data

TABLE I
SOURCE INFORMATION FOR DATA PRESENTED IN FIGS. 8 AND 9

Symbol[a]	K_{REC}[b]	NIEL[b]	ρ[b]	Type, Growth, Sample	Particle[c]	Refs.	Comments
×	1.50E-3	1.31E-5	18	n, FZ, bulk	^{60}Co gammas	[21]	Average K_{REC} for 3 samples
●	5.39E-5	1.31E-5	26	n, CZ, bulk	^{60}Co gammas	[21]	Average K_{REC} for 3 samples
□	1.47E-5	1.31E-5	25	p, FZ, bulk	^{60}Co gammas	[21]	Average K_{REC} for 3 samples
+	2.50E-5	1.31E-5	11	p, CZ, bulk	^{60}Co gammas	[21]	Average K_{REC} for 4 samples
●	1.32E-3	1.31E-5	6	n, FZ, bulk	^{60}Co gammas	[19]	
△	1.46E-3	1.31E-5	1.8	n, FZ, bulk	^{60}Co gammas	[20]	
–	4.01E-3	1.31E-5	1	n, FZ, cell	^{60}Co gammas	[18]	
■	2.36E-3	1.31E-5	1	n, CZ, cell	^{60}Co gammas	[18]	
×	1.46E-4	1.31E-5	1.3	p, FZ, cell	^{60}Co gammas	[18]	
◆	2.97E-4	1.31E-5	1.3	p, CZ, cell	^{60}Co gammas	[18]	
	2.07E-3	1.1E-5	1	n, CZ, cell	0.4-MeV e-		
	2.90E-3	3.14E-5	1	n, CZ, cell	1-MeV e-		
△	3.36E-3	6.0E-5	1	n, CZ, cell	2.7-MeV e-	[22]	
	3.94E-3	9.0E-5	1	n, CZ, cell	6.4-MeV e-		
	3.51E-3	1.2E-4	1	n, CZ, cell	16.4-MeV e-		
	3.28E-3	1.44E-4	1	n, CZ, cell	40-MeV e-		
	1.14E-4	2.0E-5	1.3	p, CZ, cell	0.6-MeV e-		
	2.47E-4	3.14E-5	1.3	p, CZ, cell	1-MeV e-		
▲	6.06E-4	6.0E-5	1.3	p, CZ, cell	2.7-MeV e-	[22]	
	9.05E-4	9.0E-5	1.3	p, CZ, cell	6.4-MeV e-		
	1.41E-3	1.2E-4	1.3	p, CZ, cell	16.4-MeV e-		
	1.79E-3	1.44E-4	1.3	p, CZ, cell	40-MeV e-		
	5.43E-5	1.63E-5	9	p, CZ, cell	0.5-MeV e-		
■	1.14E-4	3.14E-5	9	p, CZ, cell	1-MeV e-	[24]	
	1.49E-4	5.72E-5	9	p, CZ, cell	2.5-MeV e-		
▲	1.28E-3	3.14E-5	0.9	n, CZ, cell	1-MeV e-	[23]	
+	2.48E-3	3.14E-5	0.65	n, FZ, cell	1-MeV e-	[23]	
◇	1.96E-4	3.14E-5	1.3	p, FZ, cell	1-MeV e-	[23]	
	4.82E-4	5.5E-5	100	n, FZ, bulk	2.3-MeV e-		
	4.50E-4	1.0E-4	100	n, FZ, bulk	9.5-MeV e-		NIEL values at the two highest electron energies were obtained by
□	5.11E-4	1.34E-4	100	n, FZ, bulk	26-MeV e-	[27]	extrapolating information given in [17]. These approximate NIEL
	6.38E-4	1.6E-4	100	n, FZ, bulk	95-MeV e-		values are lower than those used in a previous consideration [56] of
	8.06E-4	1.8E-4	100	n, FZ, bulk	500-MeV e-		the Lugakov data [27].
	8.37E-4	1.9E-4	100	n, FZ, bulk	1.2-GeV e-		
◇	8.92E-4	7.06E-5	1.1	n, CZ, bulk	3.8-MeV e-	[28]	
◆	5.24E-4	7.06E-5	0.5	n, FZ, bulk	3.8-MeV e-	[28]	
○	3.82E-4	7.06E-5	1.2	p, CZ, bulk	3.8-MeV e-	[28]	
○	6.80E-4	7.06E-5	0.2	p, Lopex, bulk	3.8-MeV e-	[28]	Lopex-grown material has relatively low oxygen concentration
□	9.69E-3	2.83E-3	0.26	n, ?, cell	fission n	[26]	NIEL for SPR reactor is ~1.4 times that for a TRIGA reactor [30]
■	3.54E-3	2.83E-3	1.5	p, ?, cell	fission n	[26]	
△	3.73E-3	2.02E-3	< 2	n, FZ & CZ, bulk	fission n	[25]	Average K_{REC} for all samples in Fig. 6 with resistivity < 2 ohm-cm
▲	2.53E-3	2.02E-3	< 2	p, FZ & CZ, bulk	fission n	[25]	Average K_{REC} for all samples in Fig. 6 with resistivity < 2 ohm-cm
–	2.05E-3	2.83E-3	6	n, FZ, bulk	fission n	[19]	
×	1.24E-2	2.02E-3	0.4	n, FZ, diode	fission n	[29]	NIEL value is an approximation for a TRIGA reactor spectrum [2]
○	5.47E-3	3.55E-3	2.3	n, FZ, bulk	14-MeV n	[30]	K_{REC} was multiplied by 2 to compensate approximately for a
●	2.35E-3	3.55E-3	2.3	p, FZ, bulk	14-MeV n	[30]	1-year room-temperature anneal received by the samples [30]
	4.13E-3	1.5E-1	~1	p, ?, cell	0.4-MeV p+		
	4.51E-3	6.19E-2	~1	p, ?, cell	1-MeV p+		
	5.46E-3	3.24E-2	~1	p, ?, cell	2-MeV p+		
	5.92E-3	1.1E-2	~1	p, ?, cell	6.3-MeV p+		
◆	6.82E-3	5.36E-3	~1	p, ?, cell	20-MeV p+	[31]	
	5.84E-3	4.78E-3	~1	p, ?, cell	30-MeV p+		
	6.20E-3	3.3E-3	~1	p, ?, cell	65-MeV p+		
	5.37E-3	2.6E-3	~1	p, ?, cell	100-MeV p+		
	5.59E-3	1.94E-3	~1	p, ?, cell	200-MeV p+		
	1.85E-2	1.06E-2	1	n, CZ, cell	6.7-MeV p+		
	1.81E-2	7.88E-3	1	n, CZ, cell	10-MeV p+		
	2.14E-2	5.91E-3	1	n, CZ, cell	15-MeV p+		
◇	1.42E-2	5.36E-3	1	n, CZ, cell	20-MeV p+	[32] [33]	All K_{REC} values given here are corrected to low injection level
	1.15E-2	5.0E-3	1	n, CZ, cell	26-MeV p+		using results of measurements given in [32] and [33]
	1.30E-2	2.65E-3	1	n, CZ, cell	95.5-MeV p+		
	1.06E-2	2.65E-3	1	n, CZ, cell	95.5-MeV p+		
	6.51E-3	1.89E-3	1	n, CZ, cell	450-MeV p+		
	1.05E-2	1.06E-2	1	p, CZ, cell	6.7-MeV p+		
	8.41E-3	7.88E-3	1	p, CZ, cell	10-MeV p+		
+	9.21E-3	5.91E-3	1	p, CZ, cell	15-MeV p+	[32] [33]	All K_{REC} values given here are corrected to low injection level
	5.30E-3	5.36E-3	1	p, CZ, cell	20-MeV p+		using results of measurements given in [32] and [33]
	8.53E-3	5.0E-3	1	p, CZ, cell	26-MeV p+		
	5.76E-3	2.65E-3	1	p, CZ, cell	95.5-MeV p+		
×	3.56E-3	7.88E-3	0.1	p, FZ, cell	10-MeV p+	[24]	
×	5.02E-3	7.88E-3	2.5	p, FZ, cell	10-MeV p+	[24]	

[a]Both large and small symbols of the same type are employed in Figs. 8 and 9. Also, some identical symbols are used at low and high NIEL.
[b]K_{REC} is in sec^{-1} per MeV/g, NIEL is in MeV-cm^2/g, and resistivity (ρ) is in ohm-cm.
[c]The notation e- is used for electrons, p+ represents protons, and n is used for neutrons.

[18], [23] for ^{60}Co and 1-MeV electron-irradiated solar cells made from FZ and CZ material. The effects of oxygen content are evident in that regime. It is interesting to note that the damage-factor plateau values will decrease as the injection level is increased, but the high-NIEL plateaus will decrease more strongly than those at low NIEL. Fig. 7 illustrates why this will occur. At high injection levels, the recombination enhancement effects of clustered damage will no longer be operative, and isolated defects may dominate. Curtis described a defect-cluster model that predicted such behavior [34]. Recombination data and cluster modeling by Gregory [26] are also consistent with such effects.

TABLE II
RECOMBINATION ENHANCEMENT FACTOR (OR MACROSCOPIC HIGH–LOW EFFECTIVENESS RATIO) DETERMINED FROM EXPERIMENTAL RESULTS FOR VARIOUS CASES

Comparison	Sample	Type	Growth	R_{hl}	Data Sources
fission		n	CZ	4.6	[22] [23] [26]
neutrons	solar	n	FZ	3.9	[23] [26]
to 1-MeV	cells	p	CZ	19.6	[22] [24] [26]
electrons		p	FZ	18.1	[23] [26]
fission		n	CZ	4.1	[18] [26]
neutrons	solar	n	FZ	2.4	[18] [26]
to ^{60}Co	cells	p	CZ	11.9	[18] [26]
gammas		p	FZ	24.2	[18] [26]
fission		n	CZ	19.2[b]	[21][a] [25]
neutrons	bulk	n	FZ	2.7	[19] [20] [25]
to ^{60}Co		p	CZ	43.2	[21][a] [25]
gammas		p	FZ	48.7	[21][a] [25]

[a]Hewes' data [21] were scaled to 2 ohm-cm in determining R_{hl} for these cases by assuming a resistivity to the minus one-half power dependence.
[b]Hewes' data [21] for n, CZ material may have been influenced by trapping effects.

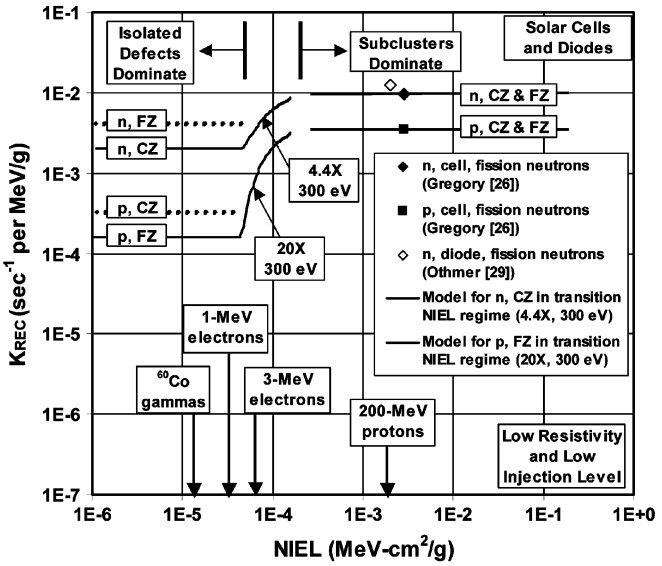

Fig. 10. Recombination damage factor versus NIEL for Si solar cells and diodes irradiated with various particles. Fission neutron data obtained by Gregory [26] and Othmer [29] are used to establish the high-NIEL values for K_{REC}. The effects of varying the oxygen concentration at low NIEL are illustrated (i.e., FZ versus CZ). This conceptual overview of recombination processes applies at low injection levels for relatively low resistivities. Results of model calculations are shown for two cases in the low-NIEL regime.

IV. SUMMARY OF MECHANISTIC FRAMEWORK

There are significant similarities between carrier generation and recombination mechanisms. For all bombarding particles with relatively low NIEL ($< 5 \times 10^{-5}$ MeV-cm^2/g), only radiation-induced isolated defects cause carrier generation and recombination. For relatively high NIEL ($>2 \times 10^{-4}$ MeV-cm^2/g), defect subclusters dominate both processes for all particles. In the transition regime for intermediate NIEL values, subclusters and isolated defects are important. In the high-NIEL regime, carrier generation in depletion regions is characterized by a single universal dark-current damage factor for all devices regardless of material and impurity type and concentration.

Carrier recombination exhibits several dependences that do not apply in the carrier generation case: a) n-type versus p-type; b) resistivity; c) injection level d) impurities (isolated defects only). For isolated defect dominance, there is a significant dependence of $K_{\rm rec}$ on material type, resistivity, and oxygen content, and a weak injection-level dependence. For defect subcluster dominance, dependences on material type and resistivity are weak, the injection-level dependence is strong, and there is no dependence on oxygen concentration. For higher injection levels and higher resistivities, $K_{\rm rec}$ decreases (Figs. 6 and 7).

A model for enhanced carrier generation was proposed [5], [6] when defect subclusters dominate. In that model, generation is assisted by charge exchange between energy levels for closely spaced defects. Enhanced *recombination* also occurs when subclusters are present, and two alternate models for that enhancement are: 1) the original Gossick model [35] (later modified by Curtis [34], [36], [37] and Gregory [26]); 2) the charge-exchange model for recombination [7]–[9], which was also invoked for enhanced generation [5], [6].

Several key questions arise with regard to the present data interpretation and physical modeling, including: 1) What is the appropriate physical model for describing enhanced carrier generation at defect subclusters? 2) What model is appropriate to account for enhanced recombination at subclusters? 3) What is the physical explanation for the difference between $K_{\rm rec}$ values at high NIEL for n- and p-type Si? 4) What is the explanation for systematic differences observed between $K_{\rm rec}$ values for solar cells and bulk material? Qualitative comments on those questions are given here.

A. Enhanced Carrier Generation at Subclusters

The Gossick model [35] and its modifications [26], [34], [36], [37] were developed to account for enhanced carrier *recombination* at defect clusters in neutral bulk material. The Gossick model basically involves the creation of a potential well for minority carriers at the cluster via trapping of majority carriers in the cluster. The defect cluster is then repulsive to majority-carrier capture and attractive to minority-carrier capture (i.e., enhanced recombination occurs in the cluster). Thermal *generation* of carriers takes place in high-field device depletion regions where potential wells and barriers at defect clusters are not present. The Gossick model appears to be inappropriate for describing the processes occurring in such regions. As noted above, Watts [5] and Gill [6] developed a charge-exchange model for enhanced generation in irradiated Si devices. Their calculations agree reasonably well with experimental results for generation enhancement factor, which supports the use of their model to account physically for subcluster effects in depletion regions.

B. Enhanced Carrier Recombination at Subclusters

Historically, the Gossick model [26], [34]–[37] was first invoked to account successfully for recombination data obtained on neutron-irradiated material and devices. Alternatively, enhanced recombination may be described using the

charge-exchange model for closely spaced defects [7]–[9], as in the generation case. A successful model must account for all experimental findings, including injection-level effects, the resistivity dependence of $K_{\rm rec}$, the difference in $K_{\rm rec}$ for n- and p-type material (discussed below), the lack of a dependence on impurities, and temperature dependences. Our initial assessment indicates that modifications and extensions of the Gossick model [26], [34], [36], [37] are more successful in accounting for those effects and dependences than the charge exchange model. The referenced cluster models have accounted successfully for most features of recombination at high NIEL, and, at least in one case, are consistent with dominance by small clusters [34].

C. Differences Between Damage Factors for n- and p-type Material

In the NIEL regime $>2 \times 10^{-4}$ MeV-cm^2/g, systematic differences are evident between $K_{\rm rec}$ values for n- and p-type material. The low-resistivity, low-injection-level results obtained by Gregory [26] for neutron-irradiated solar cells are perhaps the most accurate indicator of that difference. The n-type-to-p-type $K_{\rm rec}$ ratio derived from his data is 2.7. If we assume that subclusters in n- and p-type material behave identically in terms of enhancing carrier recombination and then examine whether the difference in $K_{\rm rec}$ values at high NIEL is due solely to the differing contributions of isolated defects in that regime, an n-type to p-type damage-factor ratio is obtained that is smaller (by a factor of $\geq$2) than Gregory's experimental value. This result indicates that cluster recombination properties are not identical in n- and p-type material. Gregory [26] explained those differences in terms of different energy levels in the cluster dominating recombination.

D. Differences Between Device and Bulk Damage Factors

Several workers [24], [26], [29], [30] have observed, and the present summary of literature data reveals, that recombination damage factors determined using solar cells (or, more generally, diodes) are systematically larger than those obtained with bulk material. Reasons considered for that difference include injection-level effects (i.e., not comparing measurements at the same injection level) [24], [26], [29], [30], trapping effects in bulk material [24], [26], [29], [30], and device effects that do not occur in bulk material [38]. Othmer [29] argued that the primary reason for differences between device and bulk damage factors at low injection levels is trapping effects in bulk samples; a secondary reason he cites is not making the comparison at the same injection level. It has also been shown [30] that device and bulk damage factors are in reasonable agreement at higher injection levels where trapping effects are unimportant. Although we favor solar cell and diode data in the present work since it is generally less susceptible to trapping effects and since measurements have been made to lower injection levels than in bulk material [26], [29], the conclusions reached herein about displacement damage mechanisms are consistent with experimental results for both bulk material *and* devices.

V. Cluster Formation

A. Experimental Evidence

Although the electrical effects of small defect clusters are not fully understood, there is a large amount of experimental evidence pointing to their existence. Perhaps the most compelling portions of that evidence are direct observations by transmission electron microscopy (TEM), which have detected defect clusters in silicon for various incident particles, including self-ions [39], medium [40] and heavy [41], [42] ions, protons [43], and even electrons [44]. The clusters detected are generally small in diameter ($< \sim 5$ nm) and have been indicated to be amorphous by microdiffraction and strong structure contrast. Studies have focused on the annealing of clusters by electron bombardment [45] and at elevated temperature [42]. Those studies show such clusters to be relatively stable at room temperature, but they anneal at temperatures ranging from slightly above room temperature to $\sim$875 K. Note that a majority of the referenced TEM experiments used *ex-situ* irradiation and often involved sample preparation between irradiation and imaging. This is further indication of the stability of these small clusters, which must at least be able to survive on the order of days based on experimental logistics.

B. Atomistic Simulations

The importance of ion implantation in semiconductor device manufacturing has led to considerable effort in atomistic simulation of displacement damage in silicon. The formation of subclusters cannot be accounted for fully using BCA Monte-Carlo calculations. High-fidelity molecular dynamics simulation techniques have been used successfully to treat the cooperative motion involved, i.e., at the ends of tracks [13], [14], [46]–[48].

The size of small disordered regions observed in the MD simulations is on the same order as that seen in TEM measurements. It is important to note that the number of atoms found in disordered regions by MD simulations is much higher ($\sim$7X) than that obtained in binary collision simulations [13]. As an illustration, a 5-keV knock-on atom was found, on average, to produce $\sim$800 displaced atoms, which is twice that expected by simply dividing the incident atom energy by a fairly liberal estimate of the displacement threshold (12.5 eV). This should not be surprising since the energy required to melt a region containing a certain number of atoms (0.524 eV/atom in Si) is much lower than that required to separately displace each of them in a well-formed lattice. Consequently, clusters may be formed more efficiently than isolated defects.

MD simulations indicate that relatively low-energy knock-ons ($<$ 500 eV) are sufficient to form clustered damage [14], which is consistent with the observation of amorphous regions following electron bombardment [44]. Damage evolution on longer timescales has also been studied using atomistic kinetic Monte-Carlo methods (e.g., [49] and [50]). Atomistic and electronic structure simulations are needed to explore further the form, evolution, and electrical effects of defect subclusters and are in progress.

VI. Discussion and Summary

We attribute the universal behavior of generation and recombination damage factors for irradiated Si at relatively high NIEL to the dominant effects of defect subclusters. For carrier generation, $K_{\rm dark}$ is independent of material and impurity type and concentration, which reveals that isolated defects are unimportant in that regime. If they were playing a role, then impurity effects would be evident. For carrier recombination, a similar situation exists. For neutron-irradiated silicon (i.e., at high NIEL), Curtis [25] demonstrated that the recombination damage coefficient at low injection levels is independent of dopant type and oxygen concentration. His data (Fig. 6) are in sharp contrast to the $K_{\rm rec}$ results for relatively low NIEL values in Figs. 8 and 9. Clusters of intrinsic defects are not expected to exhibit impurity effects because the local defect concentration is orders of magnitude greater than the impurity concentration. Curtis [34], [36] and van Lint [51] examined recombination enhancement when the same number of isolated and clustered defects is compared.

Summers [17], [52], [53] demonstrated that Si device recombination effects correlate with NIEL. For relatively high NIEL, the present recombination results are consistent with their findings in that correlation with NIEL is evident. At low NIEL, linear and quadratic dependences of the damage factor on NIEL were described [17] based on data for n- and p-type solar cells, respectively. The present work indicates that a more general framework is applicable in that regime for recombination in Si based on consideration of additional data, modeling, and simulations. We also note that Summers [17], [53] discussed some concepts that are consistent with those employed in the present analysis, including the importance of subclusters at high NIEL.

This paper has focused on the mechanisms of radiation-induced generation and recombination in bulk Si and simple devices for typical dopants and resistivities. Extensive defect engineering studies are being conducted to improve the radiation tolerance of silicon, particularly to reduce carrier removal effects in heavily irradiated particle detectors (e.g., see [54] and [55]). Consideration of the basic mechanisms responsible for those material and device hardening activities associated with carrier removal is beyond the intended scope of the present work since we are only addressing generation and recombination processes.

This paper has described a model for silicon that simultaneously accommodates defect cluster models and NIEL scaling phenomena in the same framework. The key feature is explaining that NIEL scaling works *because* of the dominant effects of defect subclusters. As NIEL increases, the number of subclusters increases linearly. Those local regions dominate carrier generation and recombination processes for particles with relatively high NIEL.

Acknowledgment

The authors would like to thank G. P. Summers for helpful communications.

References

[1] J. R. Srour, C. J. Marshall, and P. W. Marshall, "Review of displacement damage effects in silicon devices," *IEEE Trans. Nucl. Sci.*, vol. 50, no. 3, pp. 653–670, Jun. 2003.

[2] J. R. Srour and D. H. Lo, "Universal damage factor for radiation-induced dark current in silicon devices," *IEEE Trans. Nucl. Sci.*, vol. 47, no. 6, pp. 2451–2459, Dec. 2000.

[3] S. Kuboyama, H. Shindou, T. Hirao, and S. Matsuda, "Consistency of bulk damage factor and NIEL for electrons, protons, and heavy ions in Si CCDs," *IEEE Trans. Nucl. Sci.*, vol. 49, no. 6, pp. 2684–2689, Dec. 2002.

[4] Z. Li, C. J. Li, and E. Verbitskaya, "Study of bulk damage in high resistivity silicon detectors irradiated by high dose of ^{60}Co γ-radiation," *IEEE Trans. Nucl. Sci.*, vol. 44, no. 3, pp. 834–839, Jun. 1997.

[5] S. J. Watts, J. Matheson, I. H. Hopkins-Bond, A. Holmes-Siedle, A. Mohammadzadeh, and R. Pace, "A new model for generation-recombination in silicon depletion regions after neutron irradiation," *IEEE Trans. Nucl. Sci.*, vol. 43, no. 6, pp. 2587–2594, Dec. 1996.

[6] K. Gill, G. Hall, and B. MacEvoy, "Bulk damage effects in irradiated silicon detectors due to clustered divacancies," *J. Appl. Phys.*, vol. 82, pp. 126–136, Jul. 1997.

[7] W. M. Chen, B. Monemar, E. Janzen, and J. L. Lindstrom, "Direct observation of intercenter charge transfer in dominant nonradiative recombination channels in silicon," *Phys. Rev. Lett.*, vol. 67, no. 14, pp. 1914–1917, Sep. 1991.

[8] A. M. Frens, M. T. Bennebroek, A. Zakrzewski, J. Schmidt, W. M. Chen, E. Janzen, J. L. Lindstrom, and B. Monemar, "Observation of rapid direct charge transfer between deep defect levels in silicon," *Phys. Rev. Lett.*, vol. 72, no. 18, pp. 2939–2942, May 1994.

[9] A. Schenk and U. Krumbein, "Coupled defect-level recombination: Theory and application to anomalous diode characteristics," *J. Appl. Phys.*, vol. 78, no. 5, pp. 3185–3192, Sep. 1995.

[10] S. Wood, N. J. Doyle, J. A. Spitznagel, W. J. Choyke, R. M. More, J. N. McGruer, and R. B. Irwin, "Simulation of radiation damage in solids," *IEEE Trans. Nucl. Sci.*, vol. 28, no. 6, pp. 4107–4122, Dec. 1981.

[11] R. M. More and J. A. Spitznagel, "Primary recoil spectra and subcascade effects in ion bombardment experiments," *Radiat. Effects*, vol. 60, pp. 27–33, 1982.

[12] G. P. Mueller, N. D. Wilsey, and M. Rosen, "The structure of displacement cascades in silicon," *IEEE Trans. Nucl. Sci.*, vol. 29, no. 6, pp. 1293–1297, Dec. 1982.

[13] T. Diaz de la Rubia and G. H. Gilmer, "Structural transformations and defect production in ion implanted silicon: A molecular dynamics simulation study," *Phys. Rev. Lett.*, vol. 74, no. 13, pp. 2507–2510, Mar. 1995.

[14] K. Nordlund, M. Ghaly, R. S. Averback, M. Caturla, T. Diaz de la Rubia, and J. Tarus, "Defect production in collision cascades in elemental semiconductors and FCC metals," *Phys. Rev. B*, vol. 57, no. 13, pp. 7556–7570, Apr. 1998.

[15] [Online]. Available: http://www.srim.org

[16] R. A. Weller, M. H. Mendenhall, and D. M. Fleetwood, "A screened Coulomb scattering module for displacement damage computations In Geant4," *IEEE Trans. Nucl. Sci.*, vol. 51, no. 6, pp. 3669–3678, Dec. 2004.

[17] G. P. Summers, E. A. Burke, P. Shapiro, S. R. Messenger, and R. J. Walters, "Damage correlations in semiconductors exposed to gamma, electron and proton radiations," *IEEE Trans. Nucl. Sci.*, vol. 40, no. 6, pp. 1372–1379, Dec. 1993.

[18] M. Yamaguchi and O. Nagai, "Effects of impurities on gamma-irradiated silicon crystal examined by photovoltaic effect of p-n junction diode," *Jpn. J. Appl. Phys.*, vol. 11, no. 7, pp. 1016–1023, July 1992.

[19] H. J. Stein, "Comparison of neutron and gamma-ray damage in n-type silicon," *J. Appl. Phys.*, vol. 37, no. 9, pp. 3382–3384, Aug. 1966.

[20] O. L. Curtis Jr., J. R. Srour, and R. B. Rauch, "Recombination studies on gamma-irradiated n-type silicon," *J. Appl. Phys.*, vol. 43, no. 11, pp. 4638–4646, Nov. 1972.

[21] R. A. Hewes, "Recombination lifetimes in gamma-irradiated silicon," *J. Appl. Phys.*, vol. 39, no. 9, pp. 4106–4123, Aug. 1968.

[22] R. G. Downing, J. R. Carter, and J. M. Denney, "The energy dependence of electron damage in silicon," *Proc. 4th Photovoltaic Specialists Conf.*, vol. 1, pp. A-5-1–A-5-33, 1964.

[23] M. Yamaguchi, A. Khan, S. J. Taylor, M. Imaizumi, T. Hisamatsu, and S. Matsuda, "A detailed model to improve the radiation resistance of Si space solar cells," *IEEE Trans. Electron Devices*, vol. 46, no. 10, pp. 2133–2138, Oct. 1999.

[24] J. R. Srour, S. Othmer, and K. Y. Chiu, "Electron and proton damage coefficients in low-resistivity silicon," *IEEE Trans. Nucl. Sci.*, vol. 22, no. 6, pp. 2656–2662, Dec. 1975.

[25] O. L. Curtis Jr., "Effects of oxygen and dopant on lifetime in neutron-irradiated silicon," *IEEE Trans. Nucl. Sci.*, vol. 13, no. 6, pp. 33–38, Dec. 1966.

[26] B. L. Gregory, "Minority carrier recombination in neutron irradiated silicon," *IEEE Trans. Nucl. Sci.*, vol. 16, no. 6, pp. 53–62, Dec. 1969.
[27] P. F. Lugakov and I. M. Filippov, "Radiation defect clusters in electron-irradiated silicon," *Radiat. Effects*, vol. 90, pp. 297–305, 1985.
[28] D. Bielle-Daspet, "Effective recombination levels in n- and p-type silicon irradiated by 4.5 MeV electrons," *Solid-State Electron.*, vol. 16, pp. 1103–1123, 1973.
[29] S. Othmer and O. L. Curtis Jr., "Scanning electron microscope measurements of diffusion length in neutron-irradiated silicon," *IEEE Trans. Nucl. Sci.*, vol. 20, no. 6, pp. 204–208, Dec. 1973.
[30] J. R. Srour, "Stable-damage comparisons for neutron-irradiated silicon," *IEEE Trans. Nucl. Sci.*, vol. 20, no. 6, pp. 190–195, Dec. 1973.
[31] A. S. Azimov, S. M. Gorodetskii, G. M. Grigoreva, L. B. Kreinin, and A. P. Landsman, "Influence of disordered regions on the recombination in proton-irradiated p-type silicon," *Soviet Phys. Semicond.*, vol. 7, pp. 1021–1025, 1974.
[32] J. M. Denney and R. G. Downing, "Charged Particle Radiation Damage in Semiconductors, IX: Proton Radiation Damage in Silicon Solar Cells," Contract NAS5-1851, Rep. 8653-6026-KU-000, Aug. 1963.
[33] J. M. Denney, R. G. Downing, M. E. Kirkpatrick, G. W. Simon, and W. K. Van Atta, "Charged Particle Radiation Damage in Semiconductors, IV: High Energy Proton Radiation Damage in Solar Cells," Contract NAS5-1851, Rep. 8653-6017-KU-000, Jan. 1963.
[34] O. L. Curtis Jr. and J. R. Srour, "Recombination within disordered regions: influence of barrier height on recombination rate and injection level effects," *IEEE Trans. Nucl. Sci.*, vol. 20, no. 6, pp. 196–203, Dec. 1973.
[35] B. R. Gossick, "Disordered regions in semiconductors bombarded by fast neutrons," *J. Appl. Phys.*, vol. 30, no. 8, pp. 1214–1218, Aug. 1959.
[36] O. L. Curtis Jr., "The role of disordered regions in recombination of carriers in neutron-irradiated silicon and germanium," in *Lattice Defects in Semiconductors*, R. R. Hasiguti, Ed. Tokyo, Japan: Univ. Tokyo Press, 1968, pp. 333–350.
[37] O. L. Curtis Jr., "Statistics of carrier recombination at disordered regions in semiconductors," *J. Appl. Phys.*, vol. 39, no. 7, pp. 3109–3113, Jun. 1968.
[38] D. M. Bielle-Daspet and G. D. Gasset, "Bulk carrier lifetime measurement from transient diffusion photocurrent in semiconductor diodes," *Solid-State Electron.*, vol. 21, pp. 1219–1226, 1978.
[39] O. W. Holland, C. W. White, M. K. El-Ghor, and J. D. Budai, "MeV, self-ion implantation in Si at liquid-nitrogen temperature—A study of damage morphology and its anomalous annealing behavior," *J. Appl. Phys.*, vol. 68, no. 5, pp. 2081–2086, Sep. 1990.
[40] S. U. Campisano, S. Coffa, V. Raineri, F. Priolo, and E. Rimini, "Mechanisms of amorphization in ion-implanted crystalline silicon," *Nucl. Instrum. Meth. Phys. Res. B*, vol. 80/81, pp. 514–518, 1993.
[41] I. Jencic and I. M. Robertson, "Regrowth of heavy-ion implantation damage by electron beams," *Mater. Sci. Semicond. Process.*, vol. 3, pp. 311–315, 2000.
[42] S. E. Donnelly, R. C. Birtcher, V. M. Vishnyakov, and G. Carter, "Annealing of isolated amorphous zones in silicon," *Appl. Phys. Lett.*, vol. 82, no. 12, pp. 1860–1862, Mar. 2003.
[43] M. Alurralde, F. Paschoud, M. Victoria, and D. Gavillet, "The displacement damage produced in Si by 590 MeV protons," *Nucl. Instrum. Meth. Phys. Res. B*, vol. 80/81, pp. 523–527, 1993.
[44] J. Yamasaki, S. Takeda, and K. Tsuda, "Elemental process of amorphization induced by electron irradiation in Si," *Phys. Rev. B*, vol. 65, pp. 115213-1–115213-10, 2002.
[45] I. Jencic, M. W. Bench, and I. M. Robertson, "Electron-beam-induced crystallization of isolated amorphous regions in Si, Ge, GaP, And GaAs," *J. Appl. Phys.*, vol. 78, pp. 974–982, July 1995.
[46] M.-J. Caturla, T. Diaz de la Rubia, L. A. Marques, and G. H. Gilmer, "Ion-beam processing of silicon at keV energies: A molecular dynamics study," *Phys. Rev. B*, vol. 54, no. 23, pp. 16 683–16 695, Dec. 1996.
[47] G. Otto, G. Hobler, and K. Gartner, "Defect characterization of low-energy recoil events in silicon using classical molecular dynamics simulation," *Nucl. Instrum. Meth. Phys. Res. B*, vol. 202, pp. 114–119, 2003.
[48] T. Diaz de la Rubia, "Irradiation-induced defect production in elemental metals and semiconductors: A review of recent molecular dynamics studies," *Annu. Rev. Mater. Sci.*, vol. 26, pp. 613–649, 1996.
[49] L. Marques, L. Pelaz, M. Aboy, L. Enriquez, and J. Barbolla, "Microscopic description of the irradiation-induced amorphization in silicon," *Phys. Rev. Lett.*, vol. 91, no. 13, pp. 135504-1–135504-4, Sep. 2003.
[50] L. Pelaz, L. A. Marques, M. Aboy, and J. Barbolla, "Atomistic modeling of amorphization and recrystallization in silicon," *Appl. Phys. Lett.*, vol. 82, no. 13, pp. 2038–2040, Mar. 2003.
[51] V. A. J. van Lint, R. E. Leadon, and J. F. Colwell, "Energy dependence of displacement effects in semiconductors," *IEEE Trans. Nucl. Sci.*, vol. 19, no. 6, pp. 181–185, Dec. 1972.
[52] G. P. Summers, C. J. Dale, E. A. Burke, E. A. Wolicki, P. W. Marshall, and M. A. Gehlhausen, "Correlation of particle-induced displacement damage in silicon," *IEEE Trans. Nucl. Sci.*, vol. 34, no. 6, pp. 1134–1139, Dec. 1987.
[53] G. P. Summers, E. A. Burke, and M. A. Xapsos, "Displacement Damage Analogs to Ionizing Radiation Effects," *Radiat. Meas.*, vol. 24, pp. 1–8, 1995.
[54] A. Candelori (on behalf of the CERN RD50 Collaboration), "Semiconductor materials and detectors for future very high luminosity colliders," *IEEE Trans. Nucl. Sci.*, vol. 52, no. 6, pp. 2554–2561, Dec. 2005.
[55] M. Moll, "Radiation tolerant semiconductor sensors for tracking detectors," *Nucl. Instrum. Meth. Phys. Res. A*, vol. 565, pp. 202–211, 2006.
[56] C. J. Dale, P. W. Marshall, E. A. Burke, G. P. Summers, and E. A. Wolicki, "High energy electron induced displacement damage in silicon," *IEEE Trans. Nucl. Sci.*, vol. 35, no. 6, pp. 1208–1214, Dec. 1988.